Research on Structural Optimization of High-Density Wood Panel Equilibration Chamber Based on Computational Fluid Dynamics

Luxin Zhan,[a] Fuqiang He,[a,*] and Fajiang Chen [b]

To guarantee the uniformity of the flow field within an equilibration chamber during the process of hot air baking and to elevate the quality of high-density wood panels, an in-depth analysis was conducted, focusing on the impact of various factors such as the number of side air inlets in the chamber, the spacing between panel gaps, and the configuration of the bottom air inlet spacing. The aim was to optimize the structural parameters to enhance the uniformity of temperature and wind speed. The results indicated that the factors influencing the flow field uniformity within the equilibration chamber were, in descending order of importance, the number of side inlets, the spacing between the bottom inlets, and the distance between the plate gaps. In addition, the optimized hot air increased the average velocity by 0.16 m/s and the average temperature by 6.44K. The percentage of boards passing the inspection of its substandard products was only 9.2%, an improvement of 11.8 percentage points, and the average moisture content was also reduced to 8.76%. The simulation and analysis program effectively improved the uniform distribution of temperature and air velocity in the equilibration chamber and improved the quality of panel production. Therefore, the adoption of this solution helps to achieve efficient drying of wood-based panels and reduce costs.

DOI: 10.15376/biores.19.3.6747-6767

Keywords: High-density wood panels; Drying kilns; Balance chambers; Structural optimization

*Contact information: a: Guizhou University, Guiyang 550025, China; b: Guizhou Jingmu Building Materials Co., Ltd, Guiyang 550025 China; * Corresponding author: fqhe@gzu.edu.cn*

INTRODUCTION

The multi-functional wood panel is an innovative type of panel crafted primarily from wood powder. The manufacturing process involves thorough mixing and stirring of the raw material, followed by precise paving, hot pressing, sawing, and sanding to achieve the desired finish. Roasting is a key component in reducing moisture content. The process of reducing moisture content in multifunctional wood panels primarily involves introducing hot air and precisely regulating various factors within an equilibration chamber (which also can be called a kiln or a 'balance chamber'), including temperature, humidity, and air intake speed. This ensures a consistent and sustained heating and baking environment, optimizing the wood panels' moisture reduction process. The equilibration chamber considered in this work has a footprint of 30 m^2, encompassing a comprehensive setup of 24 air inlets and a solitary air outlet. The air inlets are designed to maintain a temperature of 70 °C and a wind speed of 10 m/s. In terms of production, the sheet-baking process involves accommodating over 400 sheets within this chamber, which are then left

to bake for a duration of three consecutive days. The manner and direction of the hot air circulation in the chamber affects the wind speed field and temperature field changes. The uniformity determines the drying quality and efficiency of wood-based panels. A well-conceived equilibration chamber design holds significant value, as it has the potential to substantially curtail the baking cycle for wood-based panels. This expedited process enhances the evaporation of moisture, ultimately leading to improved production efficiency and a successful reduction in moisture content. Therefore, the thorough study of the equilibration chamber's structural design is of utmost importance. In numerous studies, most of the scholars have employed Computational Fluid Dynamics (CFD) for flow field simulation. Román *et al*. (2012) optimized box dryer air distribution *via* fluid simulation, reducing moisture content variance by over 50% through enlarged inlets and diffusers. Xing *et al.* (2023) designed an adjustable air nozzle for the uneven distribution of flow field of gravure printing drying box and other problems. At the same time, to enhance the drying efficiency of the oven and ensure a more even distribution of hot air, a baffle was added to the midpoint between the oven's interior and the air inlet. Additionally, a chamfer was installed at the exit of the drying box, effectively optimizing the original oven structure. Guo *et al.* (2014) developed a simulation model that replicated the combustion chamber of a hot convection oven, aiming to analyze the temperature and flow field patterns within the burner. Their findings indicated that the burner equipped with either 19 or 21 combustion nozzles achieved the most optimal performance, optimizing both temperature distribution and airflow efficiency. Delele *et al.* (2014) optimized a dryer design *via* simulations, enlarging the inlet gap and eliminating gaps between ducts. This ensured even airflow, speeding up moisture reduction. Zdanski *et al*. (2015) employed the Ansys simulation software to investigate the width dimension and inlet flow rate of the drying kiln, aiming to achieve optimal flow uniformity throughout the entire stack. Chavan *et al*. (2021) enhanced the performance of a grain dryer through the utilization of computational fluid dynamics (CFD) analysis, optimizing the fan's size and positioning. Furthermore, they introduced orifices to intensify airflow, ultimately proposing two innovative dryer designs: a finless model and a finned variant. Hao *et al.* (2021) conducted simulations and thorough analyses of two deflector modes – parallel deflection and v-shaped deflection – within the hot air distribution system. Their findings revealed that the v-shaped deflector significantly diminished air velocity disparities, thereby enhancing the uniformity of airflow distribution to a considerable degree. Smolka *et al.* (2010) performed a comprehensive 3D CFD optimization study to examine the effects of structural parameters such as the varied shapes of fan baffles and diverse heater positions in a laboratory drying oven. The test results effectively guided the airflow distribution, significantly enhancing the temperature uniformity of the device, ultimately leading to its successful commercialization. Zhang and Deng (2017) used FLUENT software to study the effect of three structures, without deflector plate, with ordinary deflector plate and with winged deflector plate, on the moisture content of the material in the dryer. The study demonstrated an overall reduction in the water content of the wing deflector plate and an improvement in the homogeneity of the water content of the material. Zafar *et al.* (2019) conducted a numerical and parametric study of the solar oven, discovering that the incorporation of L-shaped absorber panels, in addition to internal reflectors, led to a notable enhancement in thermal performance.

Much of the current research still revolves around adjusting dryer structures or increasing inflow devices, among other methods. However, there remains a significant gap in the research pertaining to the mass production of large-scale structural equilibration

chambers capable of efficiently producing large-sized panels. Specifically, there is a lack of studies on achieving homogeneous flow fields within these chambers and optimizing their structural design. This paper addresses the issue of non-uniformity in the wind velocity and temperature fields within the equilibration chamber for wood-based panels. Utilizing CFD technology and Fluent software, the real production environment was simulated by establishing a three-dimensional model of the equilibration chamber. Through the design of orthogonal experiments and the establishment of comprehensive evaluation indices, impact of structural parameters on indoor flow uniformity and comprehensive indices was analyzed.

Based on these analyses, the structural parameters of the equilibration chamber were analyzed with the goal of enhancing the uniformity of the indoor temperature and wind velocity fields. The aim was to improve the performance of the equilibration chamber for wood-based panels, providing valuable references for subsequent design and research. This work also offers theoretical support for the enhancement of production processes in the panel industry.

EXPERIMENTAL

Equilibration Chamber Working Principle and Simulation Method

Equilibration chamber working principle

The panel kiln equilibration chamber primarily consists of a square chamber, a transmission device, and a ventilation control system. The working principle involves fixing the panel onto a bracket, which is then transported into the interior of the square chamber along the conveyor chain. Once inside, the ventilation system is activated, allowing hot air to flow into the panel baking area from the bottom and side inlets, initiating the baking process. Subsequently, the heated air is pumped out through the top air outlet, completing a cycle of heating and reuse. By monitoring the changes in temperature and humidity *via* the controller, adjustments can be made to the process parameters accordingly. Ultimately, this process achieves the desired work requirements of reducing the water content. The specific physical diagram and internal structure are shown in Fig. 1, and the main parameters of the equilibration chamber are shown in Table 1.

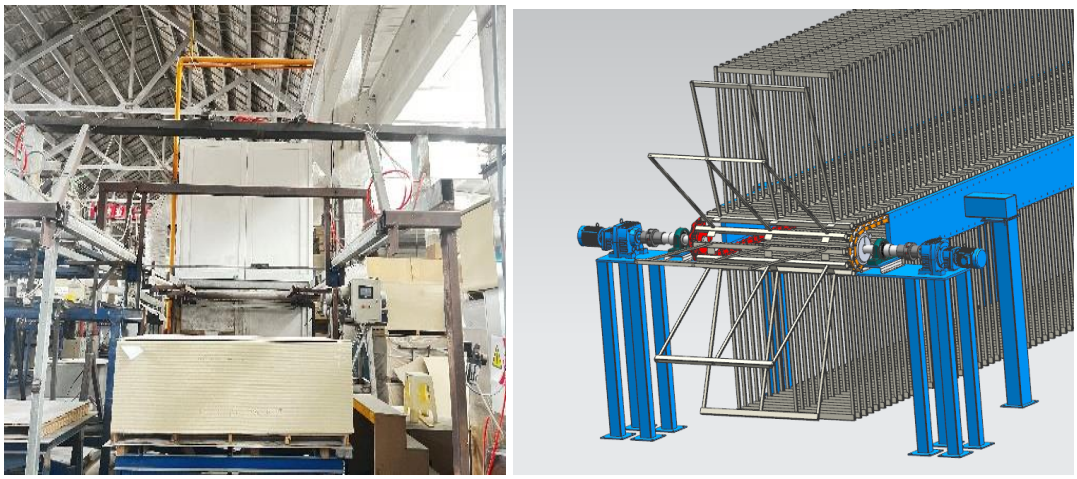

(a) (b)

Fig. 1. (a) Equilibration chamber, and (b) internal structure of the equilibration chamber

Table 1. Structural Parameters of the Equilibration Chamber

Parameter	Value (mm)
square chamber dimensions	10000 × 6000 × 3000
inlet diameter	1000 × 500
diameter of air outlet	1000 × 1000
wood panel spacing	80
bottom air inlet spacing	300
bracket size	2370 × 150 × 1353

Model Building

Physical modeling

Due to the excessively large physical size of the research object in three-dimensional modeling, the computational requirements for the established model were excessively high. Furthermore, considering the negligible impact of the internal flow field parts, a simplified modeling approach was employed. This involves deleting parts that are not involved in the flow field analysis. The specific simplification steps are outlined below. Based on the existing three-dimensional model of the equilibration chamber, it was decided to delete the internal transmission device, brackets, and other components. The original model in the overall design was a symmetrical structure, and therefore, in order to reduce the amount of calculations, the length of the model was first cut in half. After halving the structure from 5000 mm x 6000 mm x 3000 mm, the size of the bottom air inlet remained unchanged, with a total of 12 units. The top air outlet remained at 1, and in the absence of a subsequent design program, the side air inlet was excluded from the final design. A total of 100 panel models were drawn inside the equilibration chamber, with fixed positions to ensure the size remained unchanged. Finally, the entire model was set with a symmetry plane for simulation and analysis. The simplified model is shown in Fig. 2.

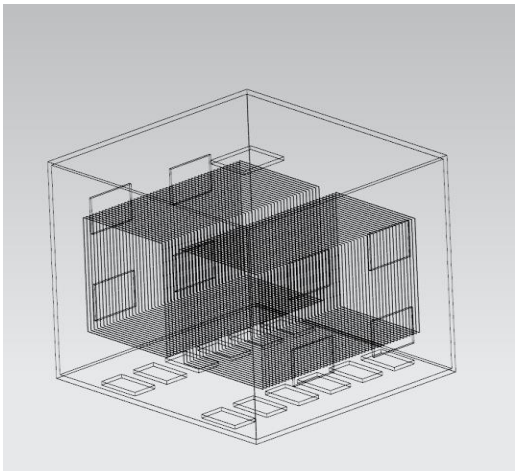

Fig. 2. Equilibration chamber model drawing

Parameterization of Control Equations and Boundary Conditions

Governing equation

During the baking of the panels, the ventilation system provides hot air at high speeds from a constant fan power source. For the purpose of simulation, the following

refined assumptions were formulated: Considering the panel as an isotropic continuous medium material, the airflow within the pores of the panel passes uniformly. The fluid medium in question is hot air, which is treated as an incompressible ideal gas, while the gravitational influence of the gas is disregarded. It is assumed that the hot air does not exchange heat transfer and components with the panel. Heat exchange between the equilibration chamber and the external environment is neglected (An *et al*. 2021; Bai *et al*. 2017; Chang *et al*. 2018). The following governing equations depend on the assumptions mentioned above.

The continuity equation, which can be also called the mass conservation equation for the fluid, is as follows,

$$\frac{\partial \rho}{\partial t}+\frac{\partial(\rho u)}{\partial x}+\frac{\partial(\rho v)}{\partial y}+\frac{\partial(\rho w)}{\partial z}=S_M \quad (1)$$

where ρ is the density of hot air ($kg \cdot m^{-3}$); u, v, w are the velocity components in x, y, z directions ($m \cdot s^{-1}$); t is the flow time of hot air (s); and S_M ($kg \cdot m^{-3} \cdot s^{-1}$) is the water vapor mass source.

The conservation of momentum equation can be expressed as follows,

$$\frac{\partial(\rho u)}{\partial t}+\mathrm{div}(\rho u \mathbf{u})=\mathrm{div}(\mu \mathrm{grad}\ u)-\frac{\partial p}{\partial x}+S_u \quad (2)$$

$$\frac{\partial(\rho v)}{\partial t}+\mathrm{div}(\rho v \mathbf{u})=\mathrm{div}(\mu \mathrm{grad}\ v)-\frac{\partial p}{\partial y}+S_v \quad (3)$$

$$\frac{\partial(\rho w)}{\partial t}+\mathrm{div}(\rho w \mathbf{u})=\mathrm{div}(\mu \mathrm{grad}\ w)-\frac{\partial p}{\partial z}+S_w \quad (4)$$

where p is the pressure (Pa); μ is the dynamic viscosity of hot air fluid ($kg \cdot m^{-1} \cdot s^{-1}$); and S_u, S_v, and S_w are the momentum source components ($N \cdot m^{-3}$).

The $k\text{-}\varepsilon$ model is widely used in fluid dynamics simulations. This is because such models are easy to code and can be utilized directly, and the computation time is short. In this paper, the following model was used for analysis,

$$\frac{\partial(\rho k)}{\partial t}+\nabla \cdot(\rho k v)=\mu \nabla \cdot \nabla k+G_k-\rho \varepsilon \quad (5)$$

$$\frac{\partial(\rho \varepsilon)}{\partial t}+\nabla \cdot(\rho \varepsilon v)=\mu \nabla \cdot \nabla \varepsilon+C_{1\varepsilon}\frac{\varepsilon}{k}G_k-C_{2\varepsilon}\rho\frac{\varepsilon^2}{k} \quad (6)$$

where G_k is the turbulence kinetic energy under the average velocity gradient ($kg \cdot m^{-1} \cdot s^{-3}$); $C_{1\varepsilon}$ and $C_{2\varepsilon}$ are the empirical constants of the model ($kg \cdot m^{-1} \cdot s^{-3}$); and $C_{1\varepsilon}$ and $C_{2\varepsilon}$ are empirical constants of the model, which are usually taken as $C_{1\varepsilon}= 1.45$, $C_{2\varepsilon} = 1.92$.

Boundary condition parameterization

The walls of the equilibration chamber were set to be adiabatic and all non-slip wall surfaces at room temperature (25 °C). The velocity inlet boundary condition was set to a hot air wind speed of 10 m/s and a temperature of 343 K. There was only one outlet in the equilibration chamber, so the outlet boundary condition was set to a pressure outlet and the value of the pressure was standard atmospheric pressure. Finally the simulation was carried out using SIMPLE algorithm based on pressure and velocity coupling with the following mathematical equation,

$$S_i=-C_0|v|^{C_1}=-C_0|v|^{(C_1-1)}v_i \quad (7)$$

where S_i is the source term of the directional (x, y, z) momentum equation; v is the velocity

magnitude (m/s); v_i is the velocity magnitude (m/s), in the i direction; and C_0 and C_1 are empirical coefficients of 0.029 and 0.6849, respectively.

Table 2. Material Parameters

Material	Density (kg·m^3)	Thermal Conductivity (W/m·K)	Specific Heat (kJ/kg·K)	Porosity
plate	1350	0.36	1.84	0.068
air	1.22	0	1	—

Irrelevance and Reliability Verification

In numerical simulation calculations of a physical model using Fluent software, a model with too few meshes or a large mesh size will result in poor mesh quality. Low mesh quality can lead to inaccurate model calculations or incorrect convergence. However, the large number and density of the meshes, coupled with the stringent hardware requirements of the computer, often results in significantly extended convergence time and heightened convergence challenges. An optimal number of meshes and the appropriate size of the results not only can favor the accuracy of the outcomes but also it can enhance the overall efficiency of the process. It is imperative to verify grid independence. Consequently, the physical model of the equilibration chamber was segmented into six distinct grid groups, comprising 800,000, 1,530,000, 2,510,000, 3,270,000, 3,520,000, and 3,840,000 grids respectively. Test calculations were conducted under identical boundary conditions, utilizing the mean temperature and average wind speed as benchmarks for validating grid independence. As can be seen from Figs. 2 to 3, with the increase in the number of grids, the temperature and wind speed were gradually decreasing and leveling off. In this work, 3.27 million grids are used for the calculations, taking into account factors such as time and computational cost.

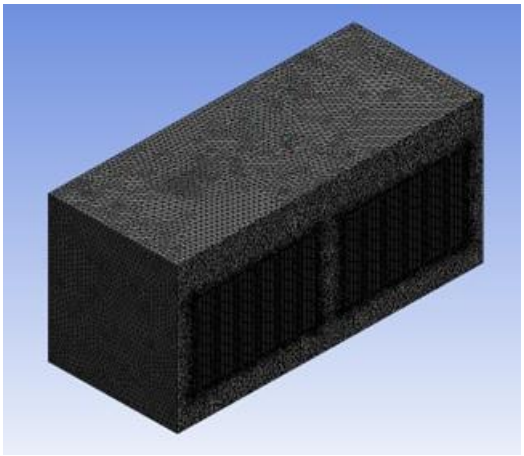

Fig. 3. Physical model meshing

After successfully conducting the grid-independence verification, to validate the credibility of the CFD flow field model and the simulation outcomes of the equilibration chamber, anemometers and temperature sensors were deployed within the chamber to conduct empirical measurements of both wind speed and temperature within its confines. By gathering the actual data from the 20 monitoring points and subsequently comparing it with the simulation data, the outcomes are presented in Figs. 5 and 6. The actual values

and the measured values at each point of the data differed, with an error range of approximately 5% to 9%. However, the overall trend of change remained consistent, indicating that the CFD model simulation possesses a certain degree of reliability and can be utilized for subsequent optimization program analysis.

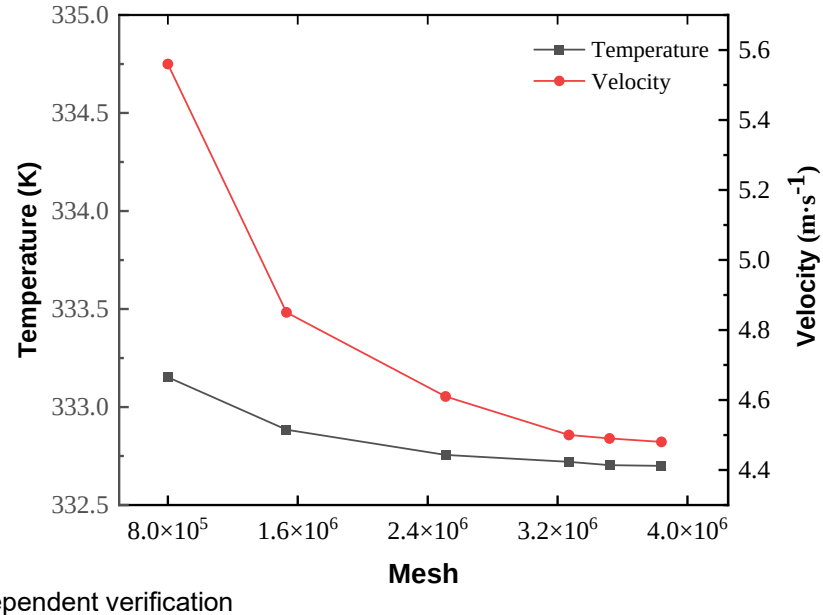

Fig. 4. Grid-independent verification

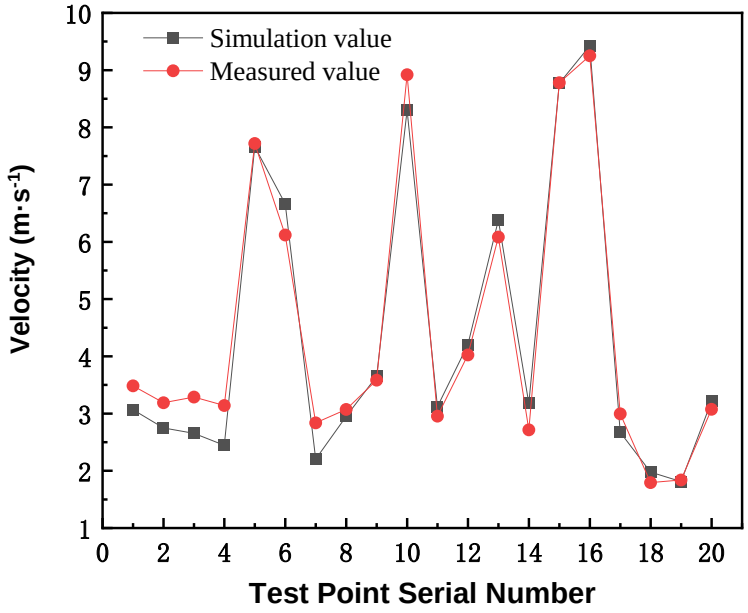

Fig. 5. Comparison of measured and simulated wind speeds at monitoring points

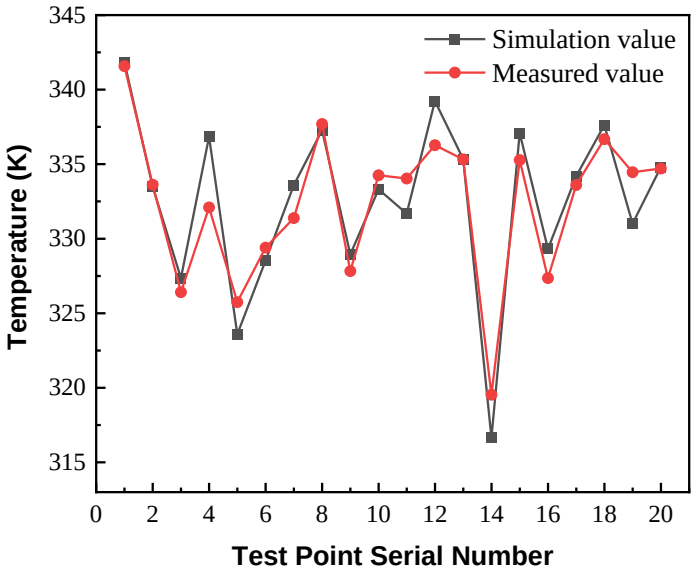

Fig. 6. Comparison of measured and simulated temperature values at monitoring points

Evaluation Indicators

The position of the air inlet and the variation in the stacking configuration of the plates will cause air flow in the equilibration chamber, thereby resulting in different velocity and temperature distributions within the chamber. Therefore, in order to analyze the flow field homogeneity inside the equilibration chamber, it is necessary to introduce corresponding evaluation indices to judge the simulation results. In Fluent software, the distribution cloud obtained by simulating the actual conditions provides the most intuitive and clearest representation of the simulation results. Due to the research needs, this paper is mainly represented by the temperature and velocity cloud maps. To quantitatively analyze the simulation data, based on the chamber's structure, a cross-section at Y=1500 mm (half-height) along the X-Z plane was selected, featuring 20 equivalent monitoring points for analysis. Introduction of the inhomogeneity coefficient in the data analysis serves as an indicator of the fluid motion's uniformity. A higher coefficient signifies greater inhomogeneity in the simulation results, whereas a lower coefficient reflects a high degree of homogeneity in the flow field. The inhomogeneity coefficient is given as,

$$C_v = \frac{S_v}{\overline{V}} = \frac{\sqrt{\frac{1}{n-1}\sum_{i=1}^{n}\left(V_i - \overline{V}\right)^2}}{\overline{V}} C \tag{8}$$

$$\mu_T = \frac{M_T}{\overline{T}} = \frac{\sqrt{\frac{1}{n-1}\sum_{i=1}^{n}\left(T_i - \overline{T}\right)^2}}{\overline{T}} T \tag{9}$$

where C_v is the velocity inhomogeneity coefficient, S_v is the standard deviation of wind speed at monitoring points (m/s), $\overline{V}$ is the mean value of wind speed at monitoring points (m/s), V_i is the wind speed at each monitoring point (m/s), μ_T is the temperature inhomogeneity coefficient, M_T is the standard deviation of temperature at monitoring points (K), $\overline{T}$ is the mean value of temperature at monitoring points (K), T_i is the temperature at each monitoring point (K), and n is the number of monitoring points.

When analyzing the flow field inside the equilibration chamber, it is necessary to consider both wind speed and temperature; hence, a combined weighted scoring method

was utilized. The principle employed is to transform the temperature and wind speed indicators into comprehensive indices of the test results for optimization analysis. According to the importance of the uniformity of the flow field distribution and its impact on the baking of the panel, the weights of temperature and wind speed were assigned 0.6 and 0.4 respectively, and the order of magnitude and scale of the indices was unified. The formula was as follows (Wang *et al*. 2023),

$$X_{I,J}^{*} = 100 \times \frac{(Y_{I,max} - Y_{I,J})}{(Y_{I,max} - Y_{I,min})} \quad (10)$$

where $X_{I,J}^{*}$ is the positive specification value of the simulation test value of the Ith indicator J, $Y_{I,J}$ is the simulation test indicator value of the Ith indicator J, $Y_{I,max}$ is the maximum value of the Ith indicator, and $Y_{I,min}$ is the minimum value of the Ith indicator.

The weighted scores for each indicator are added together to give a composite weighted score value, calculated as follows,

$$X_{J}^{**} = \sum_{I=1}^{2} W_I X_{I,J}^{*} \quad (11)$$

where $X_{J}^{**}$is the composite weighted score value of simulation test No. J, and W_I is the weight of the Ith indicator.

RESULTS AND DISCUSSION

Flow Field Analysis

Analysis of initial conditions

Initially, without side air inlets, a 300 mm bottom air inlet spacing, and a 80 mm panel gap, the wood-based panels suffered from cracking, warping, deformation, and other defects. Furthermore, the boards' average water content stood at 14%, leading to a staggering 20% defective product percentage, significantly impeding production efficiency and driving up costs. Finally, the initial conditions of the equilibration chamber were modeled and simulated, with the velocity and temperature contours in the X-Z plane captured to observe the distribution of hot air and its variations upon entering the chamber, as depicted in Fig. 7.

As hot air enters the equilibration chamber through the bottom inlet, it spreads from the center to the sides, forming a large vortex between plate rows. This reflux vortex arises due to the chamber's vast size and limited bottom airflow. Horizontal barriers prevent even dispersion, while vertical gaps allow air to concentrate at the ends. Consequently, the bottom and middle regions exhibit higher wind speeds and temperatures, while the edges and upper ends remain cooler.

In addition to this, the simulation data were derived to calculate the indicators according to the evaluation scheme described above. As shown in Table 3, the inhomogeneity coefficient under the initial conditions was high, indicating a mediocre comprehensive index score and poor overall homogeneity of the flow field. It is necessary to take measures to optimize and improve the equilibration chamber of the initial conditions in order to improve the homogeneity of the flow field, to reduce the substandard production rate, and to improve the quality of the product.

Table 3. Initial Conditions Monitoring Point Data

Average Speed ($m \cdot s^{-1}$)	Average Temperature (K)	Velocity Inhomogeneity Coefficient	Temperature Inhomogeneity Coefficient	Combined Weighted Score Value
4.45	332.72	0.4375	0.0162	67.907

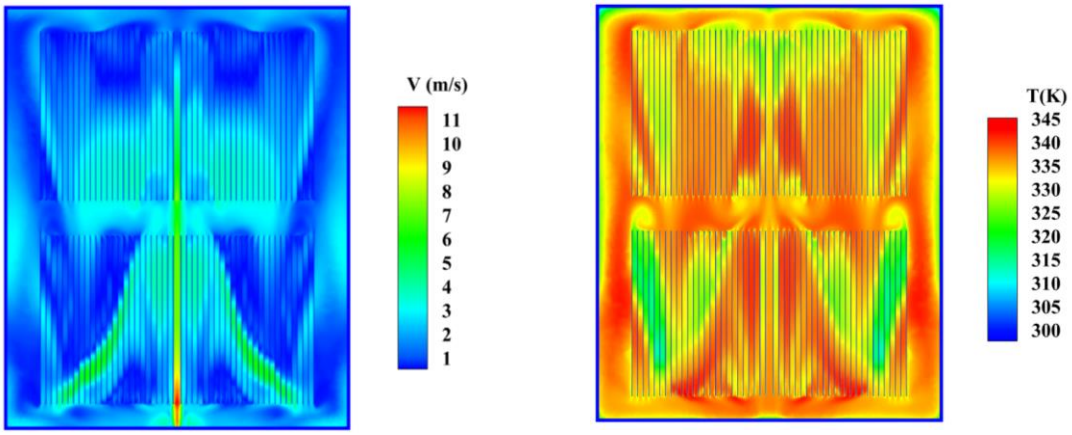

Fig. 7. Initial program wind speed and temperature cloud

Effect of Different Factors on the Flow Field

Panel gap distance

Because the panels are baked in large quantities in the equilibration chamber, the distance between the panels is one of the important factors affecting the uniformity of the whole internal flow field. Under the condition that the spacing of the bottom air inlet was 300 mm and the number of side air inlets was 0, the panel gap distances were set to 65, 70, 75, 80, and 85 mm for a one-factor sensitivity test, and the X-Z surface was selected for analysis. Figure 8 shows the effects of different panel void distances on the velocity and temperature inhomogeneity coefficients and the average velocity and temperature of the flow field inside the equilibration chamber. It can be analyzed that as the panel gap distance increases, the volume of the space between the panels through which the hot air passes also increases, although this does not have much effect on the average velocity. However, the relative ventilation velocity between the panels decreases, reducing the difference with the low-wind velocity region at the edge of the chamber, resulting in a smaller velocity inhomogeneity coefficient and a more balanced wind velocity.

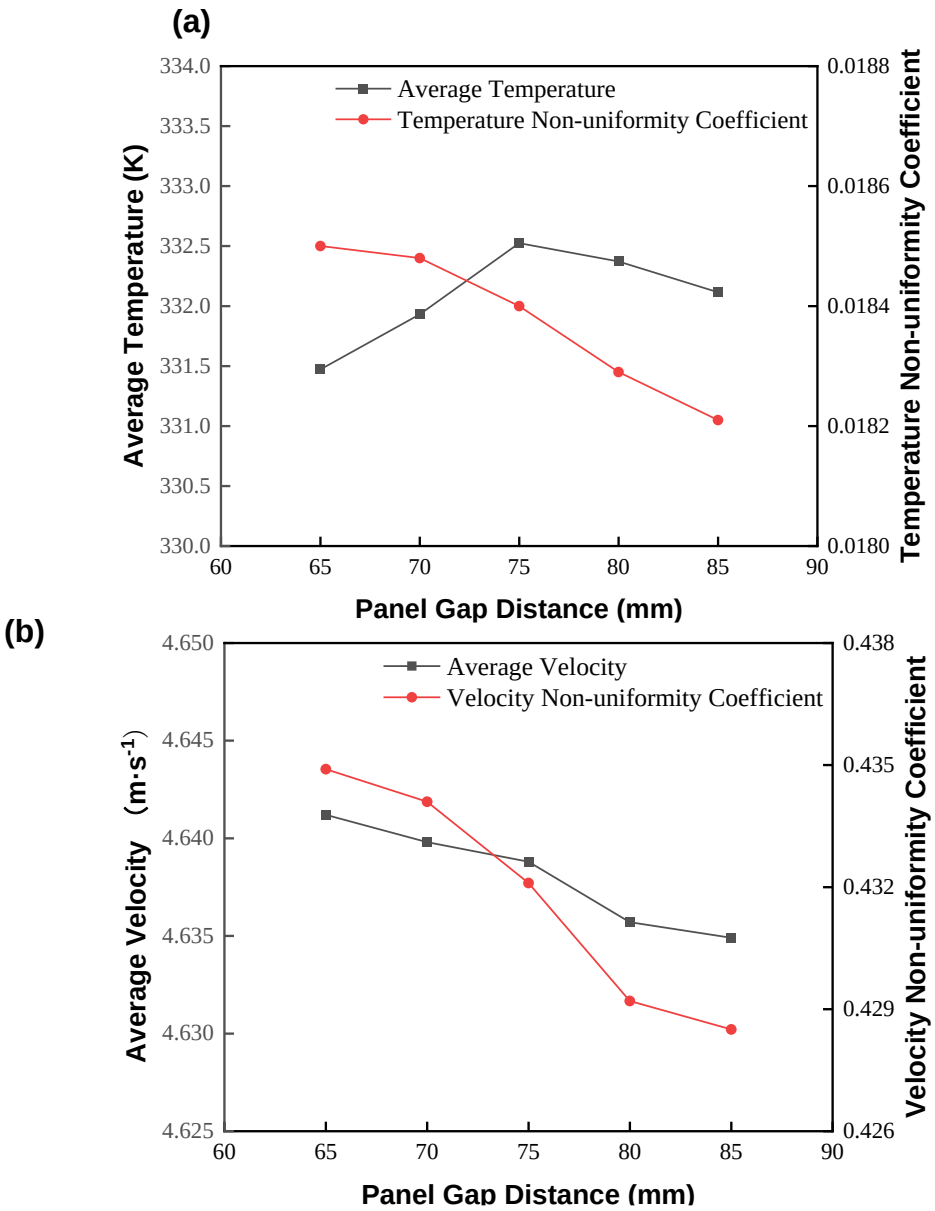

Fig. 8. (a) Effect of panel void distance on temperature inhomogeneity coefficient and mean temperature; (b) effect of panel gap distance on velocity inhomogeneity coefficient and mean velocity

In the temperature analysis, as the gap between the panels widens, the volume of hot air flowing through them increases, subjecting the panels to continuous high-intensity heat baking. This, in turn, elevates the average temperature within the chamber, while the temperature unevenness coefficient undergoes a reduction, indicating a more homogeneous thermal distribution. However, with the continuous increase of the distance of the panel gap, the wider the distribution of the panel arrangement, the edge of the low wind speed area range extends to the pile between the material, so the average temperature and wind speed exhibits a slight decline in the trend. Due to the size of the equilibration chamber, it is not possible to increase the distance between the panels without limitation, in order to be able to bake as many panels as possible at the same time in a single session. Therefore, it is determined that the range of the distance between the panels is 70 to 80 mm.

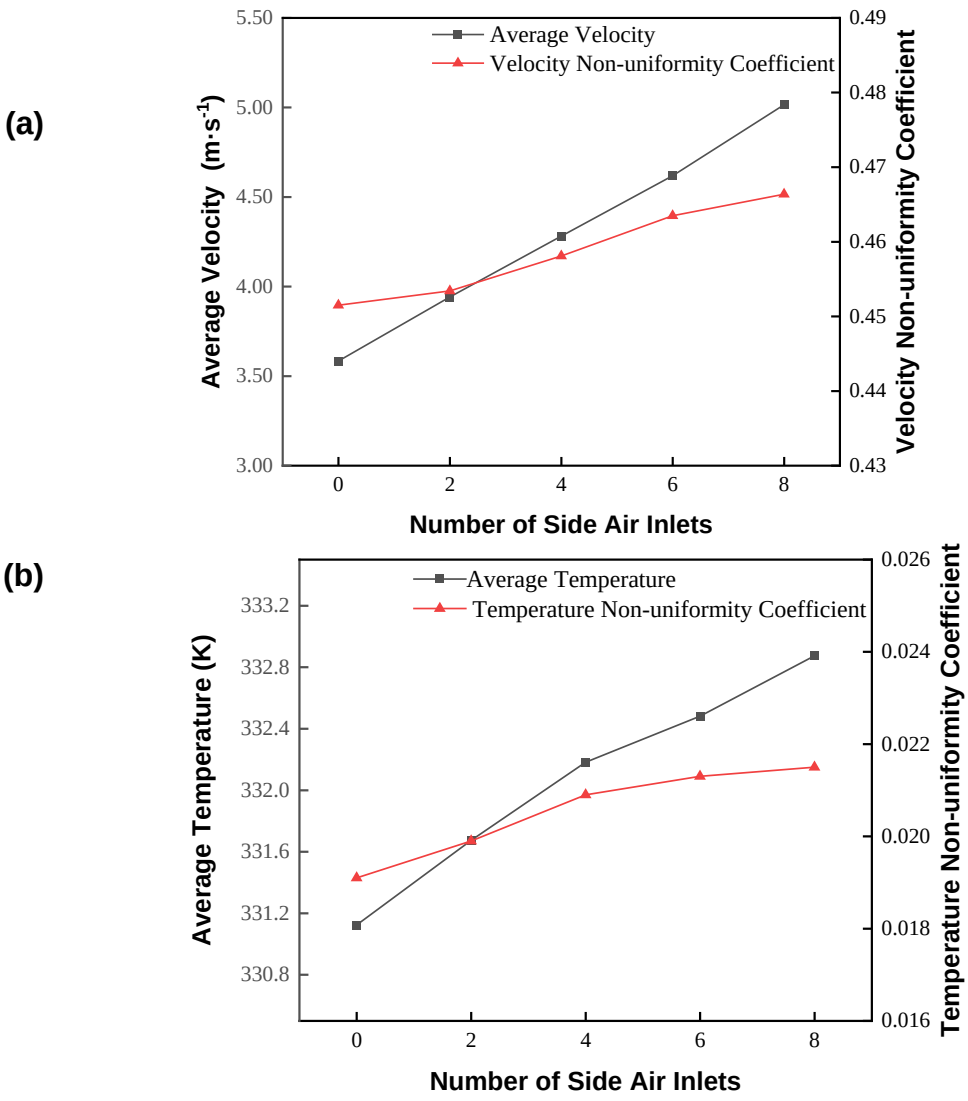

Fig. 9. (a) Effect of the number of side air inlets on the average temperature and temperature inhomogeneity coefficient; (b) effect of the number of side air inlets on the mean air velocity and velocity inhomogeneity coefficient

Number of side air inlets

When hot air is solely provided through the bottom air inlet, it travels upward along the bottom and then transfers to both sides. As it does so, the temperature and wind speed gradually decrease. This results in the edges of the panels in the chamber experiencing low-temperature and low-speed areas, while the main baking area in the middle remains significantly warmer, with faster speeds. The large difference between these areas negatively impacts the overall flow field uniformity within the chamber. Therefore, considering this factor, the number of air inlets on the side of the equilibration chamber was set as 0, 2, 4, 6 and 8 respectively, and placed symmetrically, taking the distance of the panel gap as 80 mm, and the spacing of the air inlets at the bottom as 300 mm for the one-factor simulation calculation.

As the number of air inlets increases, so does the ventilation rate, leading to a consistent upward trend in wind speed and temperature. When the hot air from the bottom reaches and comes into contact with the hot air entering through the side inlets, the

temperature and wind speed of the hot air from the side inlets are higher than that from the bottom, thus accelerating the flow dynamics inside the equilibration chamber and causing an increase in the coefficient of unevenness. In addition, the increase in the number of side air inlets also facilitates the better distribution of hot air to the upper half of the boards and the low-temperature, low-speed areas at the top of the equilibration chamber. This improvement significantly raises the overall average baking temperature, enabling the boards to reduce their moisture content more quickly and evenly, thus minimizing the likelihood of cracking in certain areas and excessive moisture content in others. The hot air stays in the chamber for too short a period of time, such that it cannot achieve the purpose of the baking to reduce the moisture content. Therefore, the combination of the above analyses determined that the number of side air inlets ranges from 0 to 4.

Bottom air inlet spacing

After analyzing the panel position and the number of side air inlets, the spacing of the bottom air inlet determines the entry position and, subsequently, the flow direction of the hot air at the bottom. It is also an important factor affecting the uniformity of the flow field in the equilibration chamber. Therefore, under the condition of a panel gap of 80 mm and zero side air inlets, the spacing of the bottom air inlet was set to 150, 200, 250, 300, and 350 mm, respectively, for the one-factor simulation calculation. As shown in Fig. 10, the change curves of the influence of different bottom inlet spacing on the average temperature, temperature inhomogeneity coefficient, average velocity and velocity inhomogeneity coefficient of the indoor flow field were simulated. It can be observed that the average air velocity and velocity inhomogeneity coefficient were gradually decreasing. This can be attributed to the fact that, as the spacing of the bottom air inlet increases, the distribution of airflow through the bottom inlet becomes wider. This wider distribution enhances the wind speed at the indoor edges of the region, while reducing the velocity in the middle region. Both of these effects tend to equalize the flow, resulting in a more stable and uniform velocity field in the equilibration chamber, with reduced differences overall. In terms of temperature, since the bottom air inlet is located closer to the edge area, it is capable of supplying more hot air to the edges. Additionally, the panels located on the outside are exposed to a more direct high-temperature airflow, thus contributing to an increase in the average temperature. However, with the further expansion of the spacing, the temperature distribution becomes more dispersed, the high temperature region shrinks, and the areas of the middle and low temperature regions increase. So the average temperature increases first and then decreases, while the temperature inhomogeneity coefficient decreases first and then increases, but the overall trend for the temperature inhomogeneity coefficient is toward a smaller value. Through the calculation and comprehensive consideration of the uniformity of the flow field inside the equilibration chamber, the preliminary determination of the bottom air inlet spacing range of 200 to 300 mm.

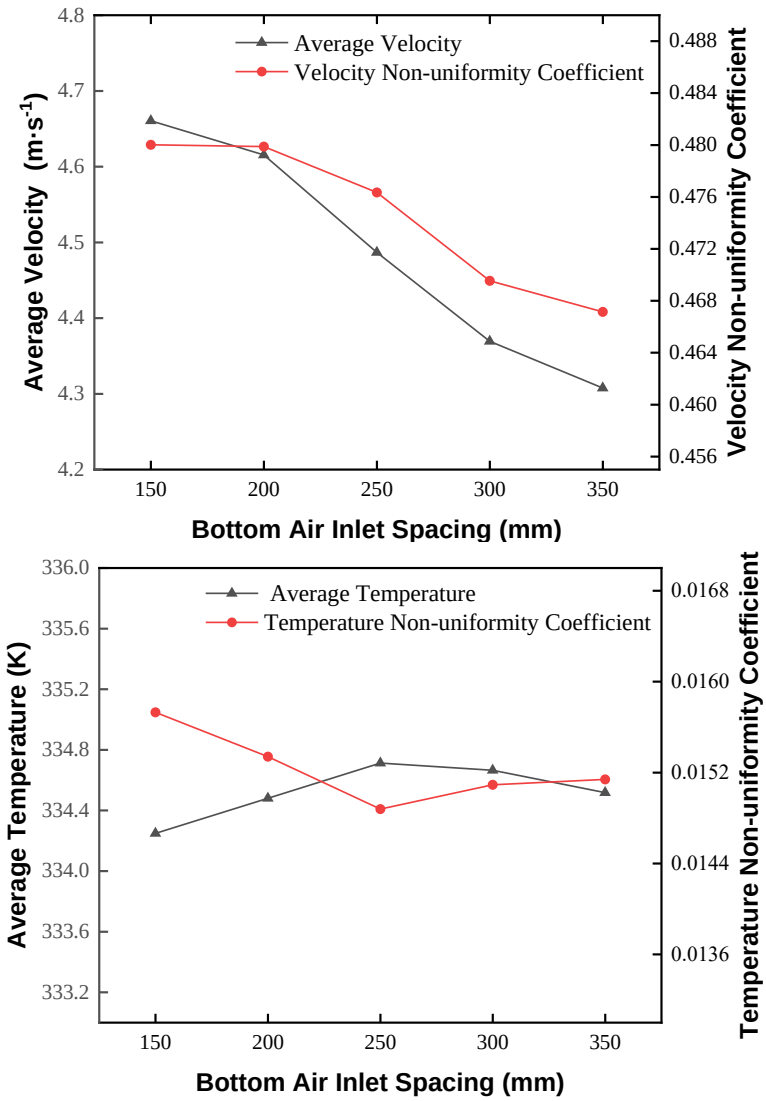

Fig. 10. (a) Effect of different bottom air inlet spacing on average temperature and temperature inhomogeneity coefficient; (b) effect of different bottom air inlet spacing on the velocity inhomogeneity coefficient of the mean anemometer

Structure and Parameter Optimization Orthogonal Experimental Design

Orthogonal test program design

The main factors affecting the uniformity of temperature and wind speed inside the equilibration chamber are the distance between the panels, the number of side air inlets and the spacing of the bottom air inlets. To obtain a better combination of structural parameters to improve the baking efficiency and flow field uniformity, orthogonal tests should be introduced to analyze the effects of different combinations of the above three variables on the flow field of the equilibration chamber. According to the analysis of the impact of different factors in the previous section to determine the range of values for the distance between the panels 70 to 80 mm, the number of side air inlets 0 to 4, the bottom air inlet spacing of 200 to 300 mm. Thus, an orthogonal test design for 3 factors with 3 levels each was created, as shown in Table 4.

The L9 (3^4) orthogonal test table was chosen to perform the simulation calculations, where L stands for the orthogonal table, 9 for the number of tests, 4 for the number of

factors, and 3 for the number of levels. The results of these simulations are presented in Tables 5 to 7. In the tables, A represents the number of side air inlets, B is the spacing of the bottom air inlet, and C is the distance between the panels.

Table 4. Orthogonal Test Factor Level Table

Level	Factors		
	Number of Side Air Inlets	Bottom Air Inlet Spacing	Panel Gap Distance
1	0	200	70
2	2	250	75
3	4	300	80

Table 5. Orthogonal Test Simulation Results

Test number	A	B	C	Velocity inhomogeneity coefficient	Temperature inhomogeneity coefficient	Combined weighted score value
1	1	1	1	0.4471	0.0190	19.3172
2	1	2	2	0.4292	0.0174	81.2500
3	1	3	3	0.4375	0.0165	67.9073
4	2	1	2	0.4532	0.0176	40.8160
5	2	2	3	0.4346	0.0165	91.1837
6	2	3	1	0.4318	0.0190	43.6718
7	3	1	3	0.4536	0.0179	31.2050
8	3	2	1	0.4537	0.0191	26.4583
9	3	3	2	0.4478	0.0189	19.4243

Table 6. Visual Analysis of Velocity Inhomogeneity Coefficients

	A	B	C
K1	1.3138	1.3539	1.3326
K2	1.3196	1.3175	1.3302
K3	1.3551	1.3171	1.3257
k1	0.4379	0.4513	0.4442
k2	0.4399	0.4392	0.4434
k3	0.4517	0.4390	0.4419
R	0.0413	0.0368	0.0069
R ordered list	1	2	3

Table 7. Visual Analysis of Temperature Inhomogeneity Coefficients

	A	B	C
K1	0.0530	0.0545	0.05447
K2	0.0531	0.0531	0.05438
K3	0.0560	0.0545	0.05327
k1	0.0177	0.0181	0.0181
k2	0.0177	0.0178	0.0181
k3	0.0187	0.0180	0.01780
R	0.0031	0.0014	0.0012
R ordered list	1	2	3

RESULTS AND DISCUSSION

Through the establishment of the above simulation model and the calculation of structural parameters *via* orthogonal testing, the simulation of reducing moisture content by baking a large quantity of boards in the equilibration chamber was realized. The speed and temperature distribution within the equilibration chamber, as well as the indexes of 20 monitoring points, were obtained. The cross-section at Y=1.5 m was chosen in order to analyze and compare the differences under each set of scenarios, and the wind speed cloud and temperature cloud of each orthogonal test scenario are shown in Figs. 11 and 12.

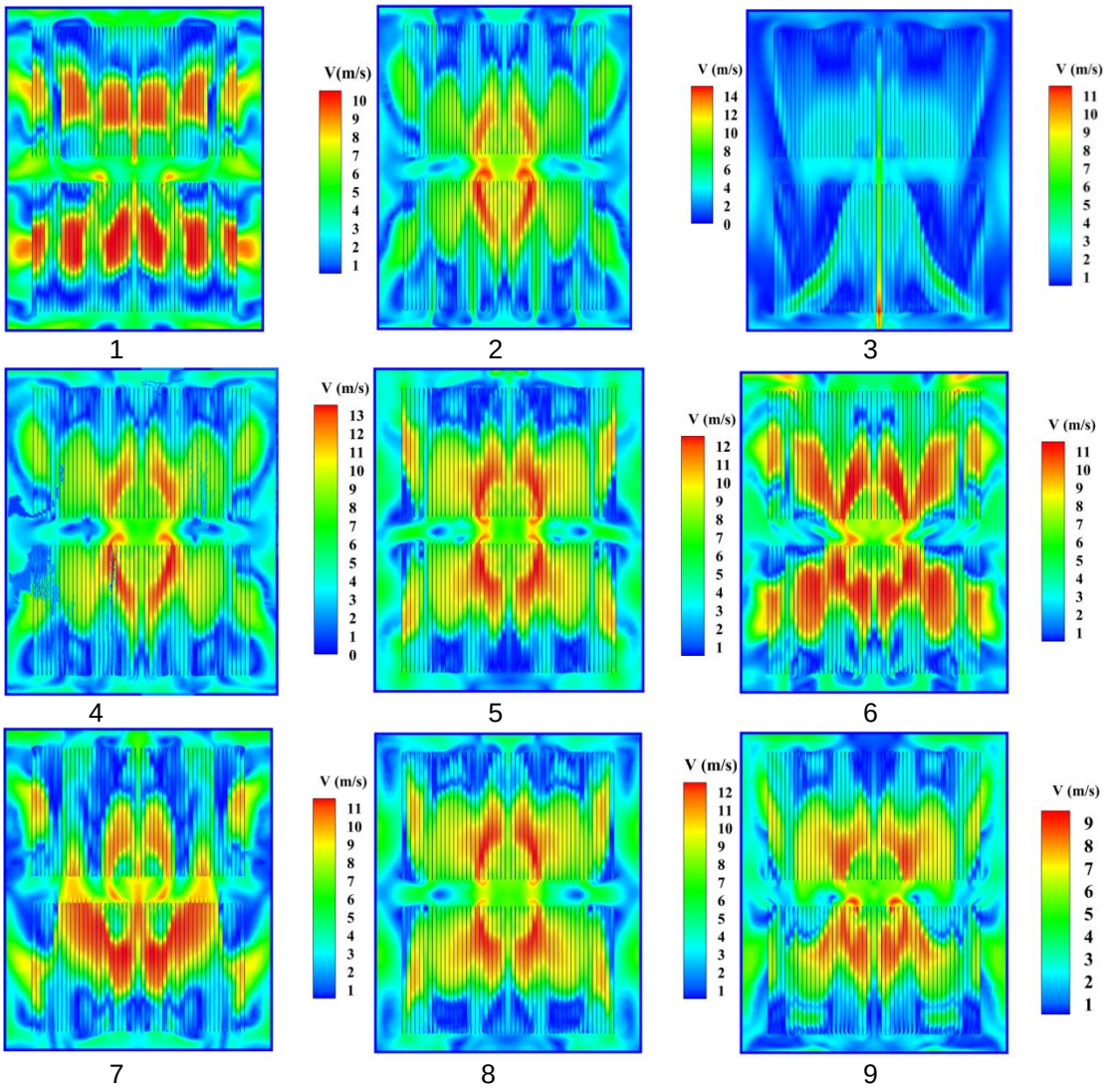

Fig. 11. Optimized scenario wind speed cloud

Compared to the initial equilibration chamber structure, all the proposed schemes exhibited variations in both velocity and temperature distributions. Among the various schemes, the velocity contour and temperature contour of Group 5 exhibited a uniform distribution of color proportions across different levels, with close gradients and smooth transitions between different colors. This indicates good internal fluidity, as well as uniform diffusion of temperature and wind speed. The analysis suggests that the

appropriate increase in the side air inlets enhanced the wind speed and temperature within the equilibration chamber, effectively mitigating the impact of wider spacing between the panels and the bottom air inlets, which tends to result in excessive temperature and airflow distribution. Consequently, the resulting unevenness has also been reduced. Analyzing the above table, K_i denotes the sum of indicators under each level of each factor, k_i denotes the average value under each level of each factor, R is the extreme deviation, and the larger the extreme deviation, the greater the influence of the factor on the indicators (Zhao *et al*. 2013). Through an intuitive analysis and ranking of the impact of three factors on the unevenness coefficient, it can be observed that the number of side air inlets had the greatest influence on the uniformity of the flow field inside the equilibration chamber, followed by the spacing of the bottom air inlets, and the distance between board gaps had the least impact.

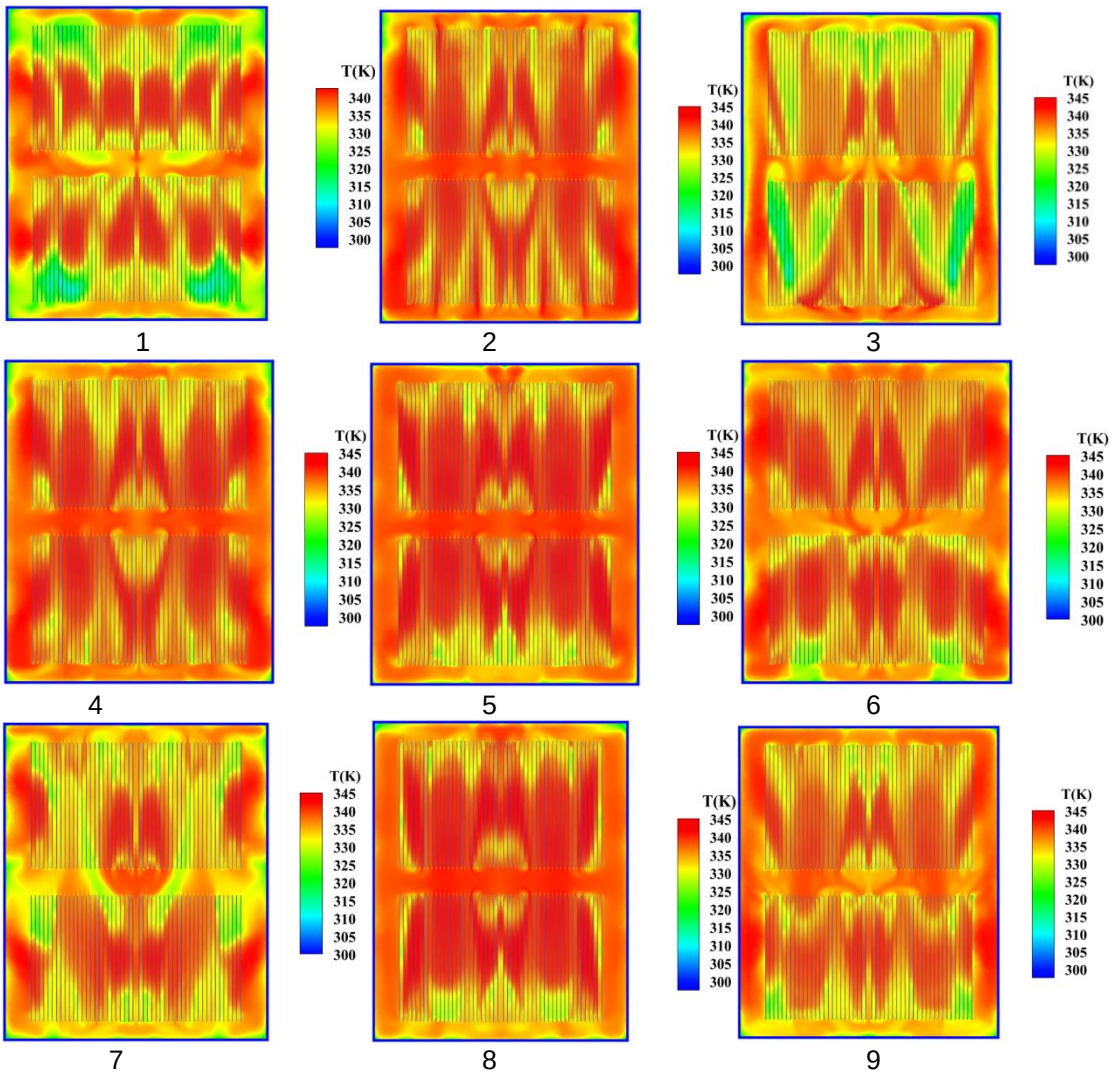

Fig. 12. Optimized solution temperature cloud

According to the results of data calculation, the optimal three-factor combination for minimizing the integrated weighted evaluation of the temperature and velocity inhomogeneity coefficients was $A_2B_2C_3$, which corresponds to the fifth group of the orthogonal test. This combination resulted in an integrated weighted average value of 91.2

for the inhomogeneity coefficient of the internal flow field in the chamber, representing a 37.6% improvement compared to the initial program. This meets the purpose and requirements of the simulation optimization.

To validate the rationality of the optimal structural parameter combination obtained from the orthogonal test, specifically, with two side air inlets, a bottom air inlet spacing of 250 mm, and a board gap distance of 80 mm, the average temperature and average wind speed within the chamber were monitored under this optimized scheme. Furthermore, multi-batch inspections were conducted on the qualification percentage and moisture content of the produced boards. Finally, a comparative analysis was made between the optimized scheme and the initial scheme to assess the differences. The test results and monitoring data are presented in Tables 8 and 9. The average speed of the optimized hot air was increased by 0.16 m/s, and the average temperature was increased by 6.44 K compared with that before the improvement. The percentage of defective boards produced under this scheme through the inspection of its sub-products was only 9.2%, which was improved by 11.8 percentage points, and the average moisture content was also reduced to 8.76%. The results indicate that the optimized scheme enhanced the fluidity of hot air, improving its effective utilization efficiency. This contributes to an increase in baking efficiency, saving on time costs, and reducing the likelihood of cracking and deformation in the boards. To further evaluate the impact of structural optimization, ten groups of panels were selected for a comparative analysis of their static bending strength, both before and after the optimization process. Static bending strength is determined as the ratio of bending moment and bending section modulus when the maximum force is applied to the panel until it breaks, methods as follows:

(1) Measuring the width and thickness of the test panel. Adjust the span between the two supports of the tester to a minimum of 20 times the thickness of the panel, and ensure that the measurement of the center distance between the supports is accurate to within 0.5 mm.

(2) The test panel should be placed on the support in such a way that its long axis is perpendicular to the support roller and its center point is aligned with the loading roller.

(3) The load is gradually increased at a constant rate, while data are recorded continuously. The amount of deformation at the midpoint of the panel is precisely measured once the maximum load is attained.

The static bending strength formula is as follows,

$$\sigma_b = \frac{3 \times F_{\mathrm{Max}} \times L}{2 \times w \times \delta^2} \quad (12)$$

where σ_b is the static bending strength of the test panel (MPa); F_{max} is the maximum load that the panel can withstand when it breaks (N); L is the distance between the two supports (mm); w is the width of the test panel (mm); and δ is the thickness of the test panel (mm).

Table 10 indicates that the optimized panels exhibited significantly higher static bending strength, thereby conclusively demonstrating the substantial improvement in panel quality achieved through the optimization.

This study has laid a robust foundation for future research avenues. Firstly, gaining deeper insights into the influence of structural parameters on the drying process of high-density wood-based panels can pave the way for further optimization of structural conditions, thereby enhancing the overall performance of the panels. Secondly, investigating the reliability of CFD technology in simulating the flow field within the equilibration chamber holds immense potential. Finally, the experimental verification of

the optimization scheme underscores its feasibility.

The proposed optimization strategy in this study has the potential to revolutionize the furniture and construction material industries. The equilibration chamber, which functions similarly to a wood drying kiln, offers valuable insights for enhancing the kiln's structural design and process parameters. Moreover, given its large-scale production and applicability to automated and batch drying kilns, it presents a viable solution.

Furthermore, its production process utilizes wood powder, minimizing reliance on virgin materials and contributing to waste reduction and the circular economy. With continued research and commercialization efforts, this high-density fiberboard could significantly contribute to transforming traditional wood drying kilns into energy-efficient and environmentally friendly systems, paving the way for a greener future in the lumber industry.

Table 8. Comparison of Flow Field Values Before and After Optimization

	Average Temperature (K)	Average Wind Speed (M/S)
Pre-Optimization	328.47	4.45
Post-Optimization	334.91	4.61

Table 9. Production Test Results

Consignment	Number of Sheets Produced	Number of Scraps	Conformity Rate (%)	Average Moisture Content (%)
2023.9.13	400	31	92.2	9.17
2023.9.20	400	46	88.5	8.48
2023.9.27	400	33	91.7	8.63

Table 10. Comparison of static flexural strength

Number	Static Bending Strength (MPa)	Mean Value of MPa
1	24.48	24.82
2	25.74	
3	25.36	
4	23.94	
5	24.58	
6	27.14	27.61
7	26.92	
8	27.67	
9	28.01	
10	28.33	

CONCLUSIONS

1. The primary and secondary factors affecting the uniformity of the temperature and air velocity flow field inside the equilibration chamber were found to be, in descending order, the number of side air inlets, the spacing of the bottom air inlets, and the distance between the panel gaps.
2. Based on the analysis of the velocity inhomogeneity coefficient and temperature inhomogeneity coefficient, the integrated weighted score value for the optimal

combination of factors indicated that with 2 side air inlets, a bottom air inlet spacing of 250 mm, and a panel gap distance of 80 mm, the internal flow field inhomogeneity coefficient within the equilibration chamber will achieve an integrated weighted average of 91.2%. This represents a significant improvement of 37.6% compared to the initial program, successfully meeting the objectives and requirements of the simulation optimization.

3. After implementing the optimization plan, a comparison between the multiple batches processed under this plan and the initial program revealed significant differences. The average hot air velocity increased by 0.16 m/s, and the average temperature rose by 6.44 K. The panels produced under this scheme have a high pass rate of 91.8% after inspection, while the average moisture content decreased to 8.76%. This indicates that the optimized solution significantly enhances hot air mobility, improving both efficiency and product quality.
4. The optimization of the structure of the equilibration chamber is limited to changing the internal structural parameters of the equilibration chamber, and only the change of the indoor flow field was analyzed. The subsequent change law of the coupling between the material change inside the sheet and the external flow field can also be considered to better explore the influence of the flow field on the water content of the sheet.
5. In the industrial realm, the equilibration chamber serves a similar purpose as a drying kiln, and thus, its research offers crucial insights for optimizing the structural and process parameters of automated, large-scale drying kilns. Furthermore, this study of wood-based panels introduces a novel, energy-efficient, and environmentally friendly approach for panel production in traditional drying kilns. This marks a transition from the inefficient drying of wood in conventional kilns to the efficient drying of panels crafted from wood powders.

REFERENCES CITED

Bai, Z., Guo, D., Li, S., and Hu, Y. (2017). "Analysis of temperature and humidity field in a new bulk tobacco curing barn based on CFD," *Sensors* 17(2), article 279. DOI: 10.3390/s17020279

Chang, T.-B., Sheu, J.-J., Huang, J.-W., Lin, Y.-S., and Chang, C.-C. (2018). "Development of a CFD model for simulating vehicle cabin indoor air quality," *Transportation Research Part D: Transport and Environment* 62, 433-440. DOI: 10.1016/j.trd.2018.03.018

Chavan, A., Vitankar, V., Shinde, N., and Thorat, B. (2021). "CFD simulation of solar grain dryer," *Drying Technology* 39(8), 1101-1113. DOI: 10.1080/07373937.2020.1863422

Delele, M. A., Mihret, Y. C., and Mellmann, J. (2023). "Performance evaluation and improvement of prototype rice husk fueled mixed flow rough rice dryer using CFD model," *Drying Technology* 41(15), 2447-2463. DOI: 10.1080/07373937.2023.2252056

Guo, H., Yan, B., Zhang, J., Liu, F., and Pei, Y. (2014). "Optimization of the number of burner nozzles in a hot blast stove by the way of simulation," *Jom* 66(7), 1241-1252. DOI: 10.1007/s11837-014-1022-z

Lv, H., Su, D., Lv, W., Lv, H., Song, K., and Du, Z. (2021). "Design of microwave hot-

airflow vibrating drying equipment for initial drying and enzymatic inactivation of fresh fruits and vegetables," *Drying Technology* 40(8), 1688-1702. DOI: 10.1080/07373937.2021.2002355

Román, F., Strahl-Schäfer, V., and Hensel, O. (2012). "Improvement of air distribution in a fixed-bed dryer using computational fluid dynamics," *Biosystems Engineering* 112(4), 359-369. DOI: 10.1016/j.biosystemseng.2012.05.008

Smolka, J., Nowak, A. J., and Rybarz, D. (2010). "Improved 3-D temperature uniformity in a laboratory drying oven based on experimentally validated CFD computations," *Journal of Food Engineering* 97(3), 373-383. DOI: 10.1016/j.jfoodeng.2009.10.032

Wang, D., Tan, L., Yuan, Y., and Lu, Y. (2023). "CFD simulation and optimization on airflow uniformity of material drying room used in steam blanching and hot-air vacuum drying equipment," *Journal of Mechanical Science and Technology* 37(10), 5463-5474. DOI: 10.1007/s12206-023-0945-0

Xing, Y. Y., Liu, P., Deng, B. Q., and Zhai, Y. H. (2023). "Study on the structure optimization and simulation analysis of oven system in gravure press," in: *Innovative Technologies for Printing and Packaging*, Vol. 991, Y. Y. Xing, P. Liu, B. Q. Deng, and Y. H. Zhai (eds.), pp. 365-374.

Zafar, H. A., Badar, A. W., Butt, F. S., Khan, M. Y., and Siddiqui, M. S. (2019). "Numerical modeling and parametric study of an innovative solar oven," *Solar Energy* 187, 411-426. DOI: 10.1016/j.solener.2019.05.064

Zdanski, P., Possamai, D., and Vaz Jr, M. (2015). "A numerical assessment of the air flow behaviour in a conventional compact dry kiln," *Journal of Applied Fluid Mechanics* 8 (3), 367-376. DOI: 10.18869/acadpub.jafm.67.222.22809

Zhang, H., and Deng, S. (2017). "Numerical simulation of moisture-heat coupling in belt dryer and structure optimization," *Applied Thermal Engineering* 127, 292-301.10. DOI: 10.1016/j.applthermaleng.2017.08.071

Zhao, X. Z., Yan, H. L., Yang, Z. X., and Xian Yu, W. L. (2013). "The study on cavitation phenomena of zoom nozzle based on orthogonal experimental and spraying mechanics," *Applied Mechanics and Materials* 468, 119-123. DOI: 10.4028/www.scientific.net/AMM.468.119

Article submitted: May 14, 2024; Peer review completed: June 22, 2024; Revised version received: June 28, 2024; Accepted: July 16, 2024; Published: July 28, 2024.
DOI: 10.15376/biores.19.3.6747-6767